Morphological control of grafted polymer films via attraction to small nanoparticle inclusions

Michael G. Opferman,[1] Rob D. Coalson,[2] David Jasnow,[1] and Anton Zilman[3,4]
[1]*Department of Physics and Astronomy, University of Pittsburgh, Pittsburgh, Pennsylvania 15260, USA*
[2]*Department of Chemistry, University of Pittsburgh, Pittsburgh, Pennsylvania 15260, USA*
[3]*Department of Physics, University of Toronto, Toronto, Ontario M5S 1A7, Canada*
[4]*Theoretical Division, Los Alamos National Laboratory, P.O. Box 1663, Los Alamos, New Mexico 87545, USA*
(Received 14 November 2011; revised manuscript received 24 August 2012; published 26 September 2012)

Control of the morphologies of polymer films and layers by addition of nanosize particles is a novel technique for design of nanomaterials and is also at the core of some important biological processes. In order to facilitate the analysis of experimental data and enable predictive engineering of such systems, solid theoretical understanding is necessary. We study theoretically and computationally the behavior of plane-grafted polymer layers (brushes) in athermal solvent, decorated with small nanoparticle inclusions, using mean field theory and coarse-grained simulations. We show that the morphology of such layers is very sensitive to the interaction between the polymers and the nanoparticles and to the nanoparticle density. In particular, the mean field model shows that for a certain range of parameters, the nanoparticles induce a sharp transition in the layer height, accompanied by a sharp increase in the number of adsorbed nanoparticles. At other parameter values, the layer height depends smoothly on the nanoparticle concentration. Predictions of the theoretical model are verified by Langevin dynamics simulations. The results of the paper are in qualitative agreement with experiments on *in vitro* models of biological transport and suggest strategies for morphological control of nanocomposite materials.

DOI: 10.1103/PhysRevE.86.031806 PACS number(s): 82.35.Np, 87.15.hp, 68.55.jd

I. INTRODUCTION

Alongside traditional bulk polymeric materials such as rubbers and plastics, thin surface films of polymers have become important in many technological applications, such as sensors, lubricant coatings, light-emitting devices, nonlinear optics, and more. Thin polymer films decorated with nanoparticles form a novel class of "responsive" composite materials allowing one to design the function and to control the morphology of the films in nanotechnological applications such as solar cells and programmable memory devices. One major technological challenge is the precise control and engineering of the properties of such composites [1–10]. In the biological context, polymerlike molecules (such as natively unfolded, disordered proteins) confined near or attached to surfaces interacting with nanosize particles (such as proteins) play important roles in many processes [11–16]. For instance, binding of certain transport proteins is thought to induce reversible morphological changes in the layer of natively unfolded proteins lining the channel of the nuclear pore complex in eukaryotic cells, and such morphological changes are at the core of the transport mechanism of this very important biological "device" [12,16–20]. In another example, binding of proteins and proteoglycans to the layer of hyaluronic acid molecules that coat cartilage cells regulates the mechanical properties of the cartilage [21]. Some of the structural and functional aspects of such biological systems can be reconstituted *in vitro* with the purpose of studying the basic mechanisms of their function, as well as for developing biomimetic nanotechnological applications, such as nanofilters and biosensors [1,22–25].

Understanding various morphologies of polymer nanoparticle mixtures at surfaces is therefore important for the predictive design of novel materials and devices as well as for the mechanistic understanding of important biological processes. These goals require predictive, quantitative theoretical understanding of the underlying physics of grafted polymers infiltrated by nanoparticles in order to compare directly with the available experimental results and make predictions in regimes that might not be directly accessible experimentally. The behavior of single-component grafted polymer films, known as "brushes," has been extensively studied, and a comprehensive theoretical framework explaining the experimental phenomena has been developed (e.g., [26–36]), providing the foundation for the present work. Brush morphologies can be controlled, for instance, by changing the solvent quality or composition, or by manipulating the direct polymer-polymer interactions [7,29–33,37–43]. Although similar to the case of mixed solvents with different properties, addition of nanoparticles to the brush is quite different physically and has been much less studied (see below). In the case of only excluded volume interactions between the polymers and the nanoparticles, Kim and O'Shaughnessy [44,45] studied theoretically the effect of particle size on their penetration and assembly into polymer brushes. Similar ideas were explored by Binder and co-workers via Brownian dynamics simulations [29]. More recently Halperin *et al*. studied the additional effect of weak attractions between the nanoparticles and polymers on the brush structure, along with the variation of the solvent quality [31]. In related systems, three-dimensional structures of mixtures of block copolymers with nanoparticles have been studied in [46,47].

In this paper, motivated by several technologically and biologically important systems [2–4,7,12,18,48,49], we study the effect of specific attractive interactions (binding) between grafted polymers and small inclusions (particles) that may infiltrate the polymer layer. In particular, we study the effect of these small nanoparticles on the film morphology, using mean field type analytical theory supported by Langevin dynamics simulations.

Our primary goal here is to establish how the properties of a polymeric layer, such as its height and composition, depend

on the concentration of nanoparticles present in it, the strength of their interaction with the polymers, and the parameters of the layer such as the grafting density. We show that such attractive interactions can result in sharp large scale changes in the layer structure, enabling global control of the polymer layer morphology and geometry, as well as nanoparticle positioning within the layer. These results are in qualitative agreement with experiments on several systems (see Discussion).

II. THE MODEL

We consider a layer of N_p flexible polymeric chains, each containing N monomers. Each chain is grafted at one end to a planar surface of area A at a distance a from its nearest neighbors. The polymer layer is in equilibrium with a solution of nanoparticles of concentration c that interact attractively with the monomers of the chains. The particles can penetrate the polymer layer, thereby changing its properties such as its density and the height above the grafting surface h (see Fig. 1 for illustration); we denote the number of nanoparticles in the layer as N_{np}. For simplicity, here we consider the nanoparticles to be of the same size as the chain monomers. With an appropriate choice of monomer size, these particles may be thought of as representing small nanoparticles (perhaps ∼1–3 nm in diameter) interacting with polymer chains, as any other small additives which may penetrate a polymer layer, or as constituents of a mixed solvent. As discussed in Sec. V, the conclusions of the mean field theory discussed below are also expected to hold for somewhat larger particles.

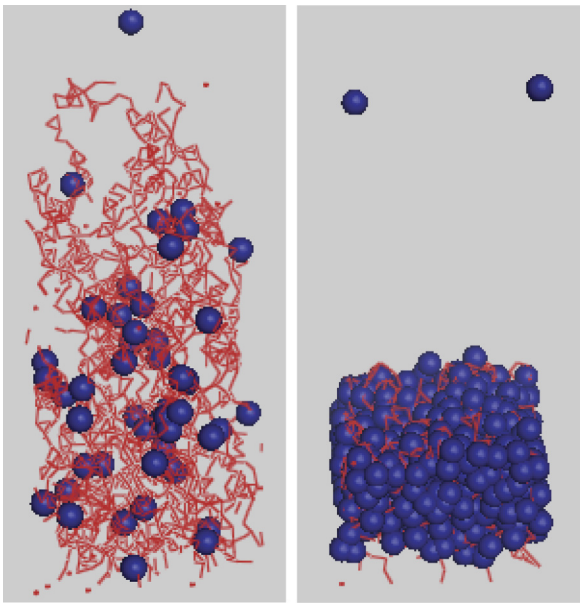

FIG. 1. (Color online) Snapshots of the Langevin simulations illustrating the collapse of the polymer layer upon addition of the nanoparticles. The nanoparticles are shown as blue spheres. Polymer chains, grafted from below onto a flat surface (not shown), are depicted in line format (i.e., their bead-spring structure is not resolved here). Left panel: The layer in the extended swollen state just below the transition; $c = 6.9 \times 10^{-5}$. Right panel: The collapsed layer packed with nanoparticles, just above the transition; $c = 2.4 \times 10^{-4}$. $\epsilon_b = 2$ and $a = 4$ for both panels. Snapshots were visualized using PYMOL [50].

The layer height h is not dictated by the polymer length alone, but is established as a result of the minimization of the total free energy of the system that depends on several salient factors: entropic stretching of the polymers, steric repulsion between the monomers, and the interactions of the polymers with the nanoparticles.

A simple mean field free energy of such a layer, per unit area in units of k_BT, can be derived, for example, using a lattice construction [27,34,39,40,43,51–53]:

$$F(\psi,h)/A = \sigma h^2/(2N) + h[\phi \ln \phi + (1-\phi-\psi) \times \ln(1-\phi-\psi) + \chi\phi\psi], \quad (1)$$

where $\sigma = N_p/A = 1/a^2$ is the polymer grafting density, $\phi = N_{np}/(Ah)$ is the density of the nanoparticles, and $\psi = N_pN/(Ah) = \sigma N/h$ is the monomer density; all lengths are measured in units of the monomer size b. The first term represents the entropic stretching of the polymers, under the assumption that the monomer density is a step function, as in the Alexander–de Gennes model [26,27,34]. For a brush without nanoparticles, the real monomer density distribution within the brush is closer to parabolic [27,33,54], but we will see that the predictions of this relatively simple extension of the Alexander–de Gennes mean field model are in very good agreement with simulations for the quantities of interest (see Sec. IV). The second term represents the translational entropy of the nanoparticles within the layer, and the third term is the correction to the translational and configurational entropies due to excluded volume effects. Together, these three terms account for the entropy of all possible arrangements of the polymers, nanoparticles, and empty sites (which are implicitly assumed to be filled with athermal solvent) [40,43,51]. Other approximations for the free energy that express similar physics are possible [34,51,52]; they result in qualitatively similar predictions. The last term in Eq. (1) describes the direct interaction between the nanoparticles and the polymers, where χ is approximately proportional to the microscopic energy of the particle-polymer interaction (see Sec. IV). In the absence of the interaction term, in the small density expansion, the free energy (1) reduces to the standard Alexander–de Gennes polymer brush [27,34]. As we will be interested also in moderately high concentration regimes, we keep the full expression for the logarithmic term, which ensures incompressibility when $\psi + \phi \to 1$, i.e., when the polymers plus the nanoparticles occupy all the available volume. Similar models have been used to study brushes in a mixture of two solvents [39,40,43]. We focus on the case of $\chi < 0$, which corresponds to attractive interactions between nanoparticles and the polymers.

The values of the variables h and ϕ are determined as sketched below. The chemical potential of the nanoparticles in the layer is, from Eq. (1),

$$\mu_{np} = \left.\frac{\partial F/A}{h\partial\phi}\right|_{h=\text{const}} = \chi\psi + \ln[\phi/(1-\phi-\psi)]. \quad (2)$$

The osmotic pressure of the layer is

$$\Pi = -\left.\frac{dF/A}{dh}\right|_{\phi h=\text{const}} = \chi\phi\psi - \frac{h\sigma}{N} - \psi - \ln(1-\phi-\psi). \tag{3}$$

Because the nanoparticles are free to diffuse between the polymer layer and the bulk solution, in equilibrium their chemical potential in the layer, μ_{np}, must be equal to the chemical potential μ_c of the nanoparticles in the solution above the layer. The osmotic pressure of the layer Π and of the solution Π_c must be equal as well. Assuming ideal solution, $\mu_c = \ln[c/(1-c)] \simeq \ln(c)$ and $\Pi_c = -\ln(1-c) \simeq c$. These two conditions determine the two unknowns: the layer height h and the concentration of the nanoparticles in the layer ϕ. These equilibrium conditions arise from the minimization of the global thermodynamic potential $\Phi(c,h,N_{np}) = F(h,N_{np}) - \mu_c(c)N_{np} + \Pi_c(c)Ah$ over layer height h and the number of nanoparticles in the layer $N_{np} = \phi hA$ when c is fixed ("grand canonical"), or the minimization of an appropriate "canonical" free energy when the total number of nanoparticles in the system is fixed instead. These two cases may correspond to different experimental situations.

III. SIMULATIONS

In order to determine whether the simple mean field theory captures the essential physics of the problem, it was augmented and verified via overdamped Langevin dynamics simulations [53,55,56]. In these simulations, the polymers are represented as chains of beads kept on the strand by finitely extensible, nonlinear, elastic (FENE) springs [34,55], which exert a force of the form

$$F_{\text{FENE}} = \frac{-kr}{1-\left(\frac{r}{\ell_{\max}}\right)^2}$$

on the nearest neighbor beads of the chain, where k is the spring constant, r is the distance between beads, and $\ell_{\max}$ is the maximum possible separation of beads, at which the FENE restoring force becomes infinitely strong. The nanoparticles are modeled as freely diffusing beads. All beads, both the monomers of the polymers and nanoparticles, interact through a pairwise 6-12 Lennard-Jones type potential [56] of the form

$$U(r) = \begin{cases} \epsilon\left[\left(\frac{b}{r}\right)^{12} - 2\left(\frac{b}{r}\right)^{6}\right] + \epsilon - \epsilon_b, & r < b \\ \epsilon_b\left[\left(\frac{b}{r}\right)^{12} - 2\left(\frac{b}{r}\right)^{6}\right], & r > b, \end{cases} \tag{4}$$

which models short-range molecular interactions. $\epsilon_b = 0$ for polymer-polymer interactions and nanoparticle-nanoparticle interactions, representing a short-range repulsion with the effective hard core diameter b and the excluded volume $\sim b^3$. For polymer-nanoparticle interactions, positive ϵ_b corresponds to attraction. Note that varying ϵ_b does not affect the excluded volume size b or the strength of the hard core repulsion interaction energy ϵ. Dynamically, in simulations each bead performs diffusion under the action of the deterministic forces from all other beads and the random thermal force [55,56]. Each chain is grafted at one end to a wall at $z = 0$, z being the perpendicular distance from the wall. The wall itself is modeled by another purely repulsive potential of the shape of Eq. (4) with $\epsilon_b = 0$ and $r = z$, centered at $z = 0$. In all simulations chains of length $N = 100$ were grafted onto a square lattice at a distance of either $a = 4b$ or $a = 3b$ from each other, in a 4×4 or 6×6 array. Periodic boundary conditions were used in the in-plane directions. The simulations were performed with two types of boundary conditions on the top of the box: one corresponding to a reservoir of nanoparticles with fixed concentration (grand-canonical ensemble with respect to particle number), the other with a fixed number of particles in the simulation box (canonical ensemble). The two different boundary conditions were found to agree in regimes of parameter space where a comparison was possible. The brush height was measured by creating time-averaged histograms of the monomer density $\rho(z)$ as a function of z [$\rho(z)$ is normalized to unity: $\int_0^\infty \rho(z)dz = 1$]. The brush height h is determined as the z value at which the monomer density becomes negligible, using the criterion that $\int_0^h \rho(z)dz = 1-\epsilon$, where ϵ is small. Specifically, for the data shown in the figures, $\epsilon = 0.000\,625$. Within the overall simulation accuracy, the results are not sensitive to the precise choice of ϵ. Once h was determined from the monomer density profile, all nanoparticles with $z < h$ were considered bound in the layer, and those with $z > h$ were considered to be in solution. The simulations and the definitions of h were tested by comparing with known cases in the absence of nanoparticles [28].

IV. RESULTS

The main result of the modeling is that the layer height, as well as its composition and morphology are very sensitive to the number of added nanoparticles and the strength of their interactions with the polymers. These results are summarized in Fig. 2 and illustrated in Fig. 1. For sufficiently strong polymer-nanoparticle interactions, increasing nanoparticle concentration from zero causes the polymer layer to compress. At still higher concentrations, the trend is reversed and further addition of nanoparticles results in the swelling of the layer.

Notably, the nature of the compactification of the polymer layer is different at high and low interaction strengths $\chi(\epsilon_b)$. For weak attraction, above a critical value χ_c, and low to moderate c, the layer height h decreases continuously with the concentration of nanoparticles c, while for $\chi < \chi_c$ and an appropriately chosen range of c, the layer undergoes a sharp change from an extended, low density state to a high density collapsed film packed with nanoparticles, as shown in Fig. 2. This abrupt collapse is accompanied by a corresponding sharp increase in the number of nanoparticles adsorbed within the layer, as shown in Fig. 1 and the lower panel in Fig. 2. The results of the mean field theory are in very good agrement with simulations, as shown in Fig. 2. The interaction parameter χ is fitted as $\chi/(b^3kT) = -8.45(\epsilon_b/kT) + 4$, consistent with the effective interaction range of $2b$ [53]; it is also closely related to the second virial coefficient of the polymer-nanoparticle interaction potential (4) [57], $\chi \simeq \frac{1}{2}\int d^3r(e^{-U(r)} - 1)$.

The heuristic physics behind this behavior is simple:Penetration of the nanoparticles increases the number of energetically favorable contacts between the polymer and the nanoparticles. This helps to overcome the entopic loss due to excluded volume interactions in the high density layer.

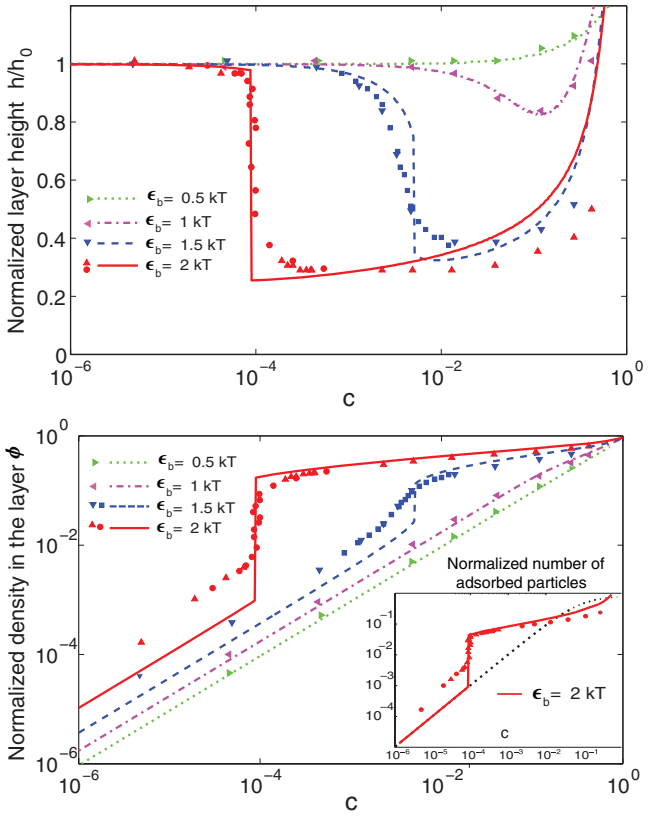

FIG. 2. (Color online) Upper panel: Layer height h normalized by the height in the absence of nanoparticles h_0 as a function of the concentration of the free nanoparticles in solution c for different interaction strengths. Lower panel: Average nanoparticle density in the layer as a function of c for the same interaction strengths as in the upper panel. The inset shows the number of adsorbed particles, per unit area, compared to a simple Langmuir adsorption isotherm (dotted line). In both panels the lines are the mean field theory ($\chi = -0.75, -4, -8, -13.5$), filled triangles correspond to grand-canonical simulations, and filled circles or squares correspond to canonical simulations. In both panels the grafting distance is $a = 4b$.

At low particle concentrations, nanoparticles penetrate the porous, swollen texture of the unperturbed layer, causing the layer to condense around them, decreasing the volume of the layer. By contrast, at higher nanoparticle concentrations, the already dense, collapsed polymer layer has to increase its volume in order to accommodate as many nanoparticles as possible. Within the Alexander–de Gennes-type mean field theory described above, the mechanism of the observed transition is characteristic of an ordinary first-order transition with discontinuous changes in densities as in a liquid-gas transition [58]. This is apparent from the analysis of the thermodynamic potential Φ: As the nanoparticle concentration c increases, the global minimum of Φ sharply switches from a high value of the layer height h to a low one (see Fig. 3).

Simulations support the general picture supplied by the mean field theory; they also provide additional information about the particle distribution within the layer. When the nanoparticle concentration is small enough so that they constitute only a small perturbation to the standard polymer

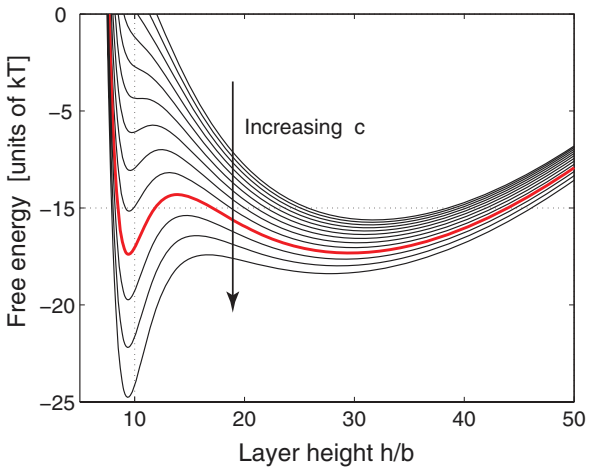

FIG. 3. (Color online) The total mean field thermodynamic potential Φ vs polymer layer height h for $a = 4$, $N = 100$, $\chi = -10$, and $10^{-4} < c < 10^{-2}$. The development of a minimum of the free energy (global thermodynamic potential) Φ at low values of h reflects the predicted transition induced by the increase in nanoparticle density. At approximately $c = 1.2 \times 10^{-3}$ (shown via the bold red line), the two minima are equal in energy.

brush, the monomer density profile is approximately parabolic as seen in Fig. 4. Although our mean field theory takes the monomer density to be constant throughout the polymer layer, the density profile obtained in simulations matches the expected behavior of a plane-grafted brush [27,32,36,54], including the presence of a depletion region near the wall and a "foot" at high z in simulations [28,59].

When the attraction between nanoparticles and polymers is sufficiently strong and the nanoparticle concentration is sufficiently high, the brush becomes highly compact, and space is almost completely filled with nanoparticles and monomers. That is, the monomer density profile becomes approximately

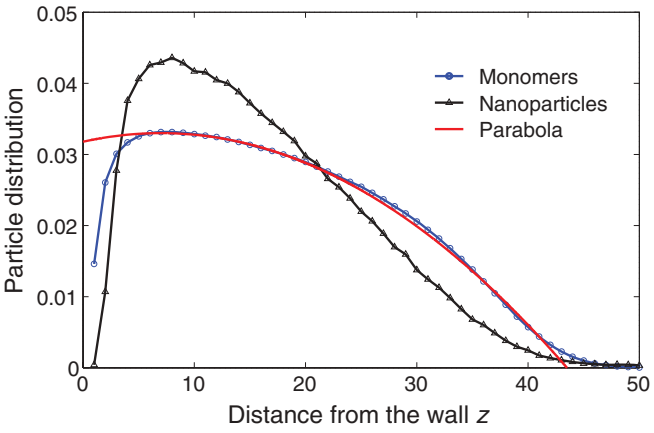

FIG. 4. (Color online) Time-averaged histograms of the monomers' and nanoparticles' distribution above the grafting surface for parameter values for which few nanoparticles are bound to the brush. The monomer distribution profile is nearly parabolic, as expected for a brush with no nanoparticles. The solid red line shows a parabola to guide the eye. Both profiles were generated for $a = 4$, $\epsilon_b = 2$, and $c = 4.2 \times 10^{-5}$. The area under both data curves is normalized to unity for presentation purposes.

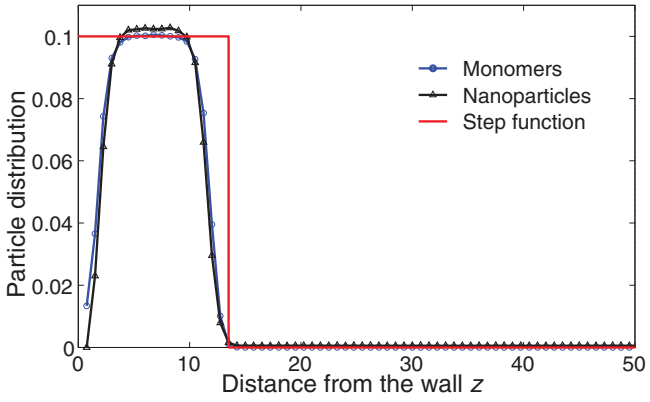

FIG. 5. (Color online) Time-averaged histograms of the monomers' and nanoparticles' distribution above the grafting surface for parameter values for which many nanoparticles are bound to the brush. The solid red line shows a step function which drops to zero at the upper brush boundary, $z = h$. Both profiles are close to step functions because monomers and nanoparticles are tightly packed as in a solid. Both profiles were generated for $a = 4$, $\epsilon_b = 2$, and $c = 2.3 \times 10^{-3}$. The area under both data curves is normalized to unity for presentation purposes.

a step function, as seen in Fig. 5. Of course in simulations the step is not infinitely sharp, but instead includes a transition region of intermediate monomer concentration. We include this intermediate region as part of the brush when calculating the height.

The corresponding nanoparticle density profiles can also be seen in Figs. 4 and 5. In both cases, the nanoparticle density profile for $z < h$ qualitatively tracks the monomer density profile consistent with the expectation that the nanoparticles in the polymer layer are bound to one or more monomers.

V. DISCUSSION

We have found that the morphology and composition of surface layers of grafted polymers can be controlled by the addition of attractive nanoparticles. In particular, we have observed a sharp transition from a low density swollen layer to a high density compact one, triggered by either an increase in the concentration of the nanoparticles or an increase in the interaction strength.

Similar models have been used in the past to describe polymer brushes in a mixture of solvents. It was found that the morphology and the height of the brush can be controlled by varying the solvent quality of one of the components of the mixed solvent, the interactions between the components, or the solvent composition. However, the changes in the brush layer were studied in the regimes where either one of the solvent components was a "bad solvent" for the polymer (repulsive interactions between nanoparticles and polymers, in our terminology) or the mixed solvent was inherently thermodynamically unstable (attraction between the nanoparticles, in our terminology). This is in contrast to the results reported here that arise solely from direct attractive interaction between the *nanoparticles and the polymers* in a stable and good solvent, without any interactions between nanoparticles themselves. In the context of previous works, this corresponds to an interesting case when both solvents in the mixture are "good solvents" for the polymer, but the brush is still unstable in a certain composition region [39–41,43,60,61].

Consideration of monomer-sized nanoparticles may be directly applicable to realistic situations, particularly if one imagines a coarse-grained approach in which one monomer is a nanoscale moiety composed of several amino acids or other chemical units. In fact, the simulations carried out in Sec. III are, by nature, coarse-grained, and, provided the polymers under consideration are sufficiently flexible, the monomer size b need not be taken on the atomic scale.

Although we present the case of monomer-size particles only, the results of this study are more broadly useful for several reasons. First, this approach is a useful framework allowing one to analyze more complicated cases, and many of the same physical arguments made here hold for particles larger than the monomer units as well. The appropriate free energy analogous to Eq. (1) can be derived on the mean field level with appropriate modifications to the lattice gas argument (or other phenomenological arguments) used to derive Eq. (1), and a similar comparison to simulation may be carried out, as will be reported elsewhere. For even larger particles, whose size exceeds the "blob" size, a characteristic length scale of the brush roughly equal to the grafting distance, additional effects not included in a simple mean field theory might become important. Such effects include corrections to the configurational entropy of the polymers arising from either adsorption onto the surface of the larger particles or meandering around them, lateral stretching of the polymers, depletion interactions between large particles induced by the smaller monomers, and crystallization of large particles [26,44–47,62–64]. The details of the density profiles might be important for precise determination of the particle distribution within the brush, and more sophisticated theories such as self-consistent field theory (SCFT) might be needed [27,30,32,41,44,54,60,61,65]. However, preliminary simulations with larger nanoparticles show that the qualitative predictions of the simple mean field theory hold even for larger nanoparticles. This is in accord with the general understanding that for particles of size smaller than the blob size, additional effects such as the lateral polymer stretching are subdominant [29,44,45,63,66]. A systematic discussion of the effects of the particle size and the above mentioned issues will be presented elsewhere. The fact that the simulations support the simple mean field picture presented here suggests that the Alexander–de Gennes-type theory does capture the essential complexity of the problem, but it should be noted that preliminary SCFT calculations and simulations with particle volumes greater than unity (relative to monomer volume) suggest that the strict discontinuity in brush height predicted by the Alexander–de Gennes model may, in the true thermodynamics of the system, be sharp but continuous [60,61]. Further discussion of various levels of theory and additional Langevin simulations will be presented elsewhere.

Our results suggest strategies for the control of morphologies of composite materials for practical applications. The insights from the model also inform future analysis of biological systems such as interactions of unfolded polypeptides with nanoparticlelike objects such as small proteins and provide resolution for existing controversies [18,19]. One particular

motivation for our work is the controversy regarding possible morphological changes in the layers of natively unfolded constituents of the nuclear pore complex induced by the binding of other folded proteins [18,19]. Although our model, in its present form, is not directly applicable to this system due to the relatively large nanoparticles involved in the latter, the results are qualitatively consistent with the observed behavior. In addition, it provides a foundation on which to construct more elaborate models. Finally, the strong dependence of the number of the nanoparticles in the layer on their concentration in the bulk may have important implications for the estimation of the binding affinities to flexible objects such as unfolded proteins [11,67].

ACKNOWLEDGMENTS

The authors thank Roderick Lim, Yitzhak Rabin, Michael Rexach, and Paul Welch for helpful discussions. A.Z. acknowledges the support from NSERC and DOE. R.D.C. acknowledges financial support from NSF Grant No. CHE-0750332. This research was supported in part by the University of Pittsburgh Center for Simulation and Modeling through the supercomputing resources provided. Part of the simulations were performed on the GPC supercomputer at the SciNet HPC Consortium. SciNet is supported by the Canada Foundation for Innovation under the auspices of Compute Canada, the Government of Ontario, Ontario Research Fund, and the University of Toronto.

[1] W. Senaratne, L. Andruzzi, and C. K. Ober, Biomacromolecules **6**, 2427 (2005).
[2] E. P. K. Currie, W. Norde, and M. A. C. Stuart, Adv. Colloid Interface Sci. **100–102**, 205 (2003).
[3] I. Luzinov, S. Minko, and V. Tsukruk, Soft Matter **4**, 714 (2008).
[4] A. C. Balazs, T. Emrick, and T. P. Russell, Science **17**, 1107 (2006).
[5] R. J. Tseng, J. Huang, J. Ouyang, R. B. Kaner, and Y. Yang, Nano. Lett. **5**, 1077 (2005).
[6] S. J. Green, J. J. Stokes, M. J. Hostetler, J. Pietron, and R. W. Murray, J. Phys. Chem. B **101**, 2663 (1997).
[7] L.-M. Chen, Z. Hong, G. Li, and Y. Yang, Adv. Mater. **21**, 1434 (2009).
[8] J. Ouyang, C.-W. Chu, C. R. Szmanda, L. Ma, and Y. Yang, Nature Mater. **3**, 918 (2004).
[9] A. Boker, J. He, T. Emrick, and T. Russell, Soft Matter **3**, 1231 (2007).
[10] I. Galaev and B. Mattiasson, Trends Biotechnol. **17**, 335 (1999).
[11] S. S. Patel, B. J. Belmont, J. M. Sante, and M. F. Rexach, Cell **129**, 83 (2007).
[12] M. Stewart, Nat. Rev. Mol. Cell Biol. **8**, 195 (2007).
[13] M. Stewart and S. M. Liu, J. Mol. Biol. **349**, 515 (2005).
[14] V. N. Uversky, Protein Sci. **11**, 739 (2002).
[15] D. Ron and P. Walter, Nat. Rev. Mol. Cell Biol. **8**, 519 (2007).
[16] S. Wente and M. Rout, Cold Spring Harbor Perspect. Biol. **2**, a000562 (2010).
[17] S. Frey and D. Gorlich, Cell **130**, 512 (2007).
[18] R. Lim, B. Fahrenkrog, J. Köser, K. Schwarz-Herion, J. Deng, and U. Aebi, Science **318**, 640 (2007).
[19] N. Eisele, S. Frey, J. Piehler, D. Görlich, and R. Richter, EMBO Rep. **11**, 366 (2010).
[20] T. Kustanovich and Y. Rabin, Biophys. J. **86**, 2008 (2004).
[21] T. Hardingham and H. Muir, Biochim. Biophys. Acta **279**, 401 (1972).
[22] P. Kohli, C. Harrell, Z. Cao, R. Gasparac, W. Tan, and C. R. Martin, Science **305**, 984 (2004).
[23] Y. Caspi, D. Zbaida, H. Cohen, and M. Elbaum, Nano Lett. **8**, 3728 (2008).
[24] T. Jovanovic-Talisman, J. Tetenbaum-Novatt, A. S. McKenney, A. Zilman, R. Peters, M. P. Rout, and C. B. T., Nature (London) **457**, 1023 (2009).
[25] S. Kowalczyk, L. Kapinos, T. Blosser, T. Magalhães, P. van Nies, R. Lim, and C. Dekker, Nat. Nanotechnol. **6**, 433 (2011).
[26] P. G. de Gennes, Macromolecules **13**, 1069 (1980).
[27] S. T. Milner, T. A. Witten, and M. E. Cates, Macromolecules **21**, 2610 (1988).
[28] M. Murat and G. S. Grest, Macromolecules **22**, 4054 (1989).
[29] J. Yaneva, D. Dimitrov, A. Milchev, and K. Binder, J. Colloid Interface Sci. **336**, 51 (2009).
[30] C. Yeung, A. Balazs, and D. Jasnow, Macromolecules **26**, 1914 (1993).
[31] A. Halperin, M. Kröger, and E. Zhulina, Macromolecules **44**, 3622 (2011).
[32] E. Zhulina, O. Borisov, V. Pryamitsyn, and T. Birshtein, Macromolecules **24**, 140 (1991).
[33] J. Field, C. Toprakcioglu, R. Ball, H. Stanley, L. Dai, W. Barford, J. Penfold, G. Smith, and W. Hamilton, Macromolecules **25**, 434 (1992).
[34] K. Binder, T. Kreer, and A. Milchev, Soft Matter **7**, 7159 (2011).
[35] B. Mognetti, P. Virnau, L. Yelash, W. Paul, K. Binder, M. Müller, and L. MacDowell, J. Chem. Phys. **130**, 044101 (2009).
[36] S. Milner, Science **251**, 905 (1991).
[37] O. Borisov, E. Zhulina, B. Mattiasson, and I. Galaev, *Smart Polymers: Applications in Biotechnology and Biomedicine*, edited by B. Mattiasson and I. Galaev (CRC Press, Taylor and Francis, Boca Raton, FL, 2007), p. 53.
[38] J. Marko, Macromolecules **26**, 313 (1993).
[39] T. Birshtein and Y. Lyatskaya, Colloids Surf. A **86**, 77 (1994).
[40] T. Birshtein and Y. Lyatskaya, Macromolecules **27**, 1256 (1994).
[41] T. Birshtein, A. Mercurieva, and E. Zhulina, Macromol. Theory. Simul. **10**, 719 (2001).
[42] Y. Lyatskaya and A. Balazs, Macromolecules **30**, 7588 (1997).
[43] P. Lai and A. Halperin, Macromolecules **25**, 6693 (1992).
[44] J. U. Kim and B. O'Shaughnessy, Macromolecules **39**, 413 (2006).
[45] J. U. Kim and B. O'Shaughnessy, Phys. Rev. Lett. **89**, 238301 (2002).
[46] J. Huh, V. Valeriy, and A. Balazs, Macromolecules **33**, 8085 (2000).
[47] V. Pryamitsyn and V. Ganesan, Macromolecules **39**, 8499 (2006).

[48] R. Lim, U. Aebi, and B. Fahrenkrog, Histochem. Cell Biol. **129**, 105 (2008).
[49] S. S. Patel, B. J. Belmont, J. M. Sante, and M. F. Rexach, Cell **129**, 83 (2007).
[50] The PYMOL Molecular Graphics System, Version 1.3, Schrödinger, LLC, 2010.
[51] P. J. Flory, *Principles of Polymer Chemistry* (Cornell University Press, New York, 1953).
[52] P. de Gennes, *Scaling Concepts in Polymer Science* (Cornell University Press, New York, 1979).
[53] M. Opferman, R. Coalson, D. Jasnow, and A. Zilman, arXiv:1110.6419.
[54] C. Wijmans, J. Scheutjens, and E. Zhulina, Macromolecules **25**, 2657 (1992).
[55] K. Binder, *Monte Carlo and Molecular Dynamics Simulations Polymer* (Oxford University Press, New York, 1995).
[56] A. R. Leach, *Molecular Modelling: Principles and Applications*, 2nd ed. (Pearson Education Ltd., Harlow, 2001).
[57] M. Doi and S. F. Edwards, *The Theory of Polymer Dynamics* (Oxford University Press, Oxford, 1988).
[58] R. Pathria, *Statistical Mechanics*, 2nd ed. (Elsevier, Oxford, 1996).
[59] S. T. Milner, J. Chem. Soc., Faraday Trans. **86**, 1349 (1990).
[60] T. Birshtein, V. Amoskov, L. Klushin, A. Mercurieva, A. Polotsky, and P. Iakovlev, *Macromolecular Symposia* (Wiley Online Library, 2003), Vol. 191, pp. 51–58.
[61] V. Amoskov, T. Birshtein, and A. Mercurieva, Macromol. Theory Simul. **15**, 46 (2006).
[62] T. Biben and J. P. Hansen, Phys. Rev. Lett. **66**, 2215 (1991).
[63] F. Solis and H. Tang, Macromolecules **29**, 7953 (1996).
[64] H. Lekkerkerker and R. Tuinier, *Colloids and the Depletion Interaction*, Lecture Notes in Physics (Springer, Heidelberg, 2011), pp. 109–129.
[65] A. Milchev, S. Egorov, and K. Binder, J. Chem. Phys. **132**, 184905 (2010).
[66] O. A. Guskova, S. Pal, and C. Seidel, Europhys. Lett. **88**, 38006 (2009).
[67] J. Tetenbaum-Novatt, L. E. Hough, R. Mironska, A. S. McKenney, and M. P. Rout, Molecular & Cellular Proteomics **11**, 31 (2012).